

## Supplementary Information

Here we first describe the algorithms used to simulate HD 209458b's hydrogen exosphere, we then describe the detailed setup used in the numerical experiments, and finally we investigate the effects of changing some model parameters.

### The simulation algorithm

In what follows, the coordinate system used is centered at the planet and has its  $x$ -axis toward the star, a  $z$ -axis perpendicular to the planet's velocity, and a  $y$ -axis opposite the planet's orbital velocity,  $v_p$ , that completes the right handed system.

The outer boundary of the simulation domain is the box  $x_{\min} \leq x \leq x_{\max}$ ,  $y_{\min} \leq y \leq y_{\max}$ , and  $z_{\min} \leq z \leq z_{\max}$ . The inner boundary is a sphere of radius  $R_0$ .

At the start of the simulation the domain is empty of particles. Then hydrogen meta-particles are launched from the inner boundary at a rate of 600 meta-particles per second. Each meta-particle corresponds to  $N_m$  hydrogen atoms. The location on the inner boundary of each launched particle is randomly drawn with probability proportional to the local hydrogen exobase density. The velocity of each launched particle is randomly drawn from a probability distribution proportional to

$$(\mathbf{n} \cdot \mathbf{v}) e^{-a|\mathbf{v}|^2},$$

where  $\mathbf{n}$  is the local unit surface normal,  $\mathbf{v}$  is the velocity of the particle, and  $a = m/(2kT)$ ,  $m$  is the mass of a neutral,  $k$  is Boltzmann's constant, and  $T$  is the temperature (at the exobase position). Note that the distribution used is not a Maxwellian, but the distribution of the flux through a surface (the exobase), given a Maxwellian distribution at the location<sup>1</sup>. The number flux through the surface is  $n/\sqrt{4\pi a}$ , where  $n$  is the inner boundary hydrogen density, for a total production rate of  $nR_0^2\sqrt{8\pi kT/m}$  s<sup>-1</sup>. After an hydrogen atom is launched from the inner boundary, we numerically integrate its trajectory with a time step of 25 seconds.

Before each time step we also fill the  $x$ -axis shadow cells (cells just outside the simulation domain) with proton meta-particles of the same weight as for hydrogen,  $N_m$ . After each time step the shadow cells and the obstacle region are emptied of protons. The protons are drawn from a Maxwellian distribution with temperature  $T_{\text{sw}}$  and bulk velocity  $v_{\text{rel}}$ . The relative velocity at the planet,  $v_{\text{rel}}$ , is related to the stellar wind velocity and the planet's orbital velocity by  $v_{\text{rel}}^2 = v_{\text{sw}}^2 + v_p^2$ . This ensures that a uniform stellar wind eventually builds up in the simulation domain, outside the obstacle. The boundary conditions in the  $y$ - and  $z$ -directions are periodic.

Between time steps, the following events can occur for an exospheric atom

- Collision with an UV photon. Following Hodges<sup>2</sup> this occurs as an absorption of the photon ( $\Delta v$  opposite the sun direction) followed by isotropic reradiation ( $\Delta v$  in a random direction).

From Hodges<sup>2</sup> we use a velocity change  $\Delta v = 3.27$  m/s. The collision rate is zero if the particle is in the shadow behind the planet.

- Photoionization by a solar photon occurs at a rate of  $\tau_i$  when an exospheric hydrogen atom is outside the optical shadow behind the planet, and then the meta-particle is removed from the simulation.
- Charge exchange with a stellar wind proton. If the hydrogen atom is outside the obstacle it can charge exchange with a solar wind proton, producing an ENA. This is done using the DSMC method described in the next section. We define the obstacle by the conic surface  $(X, \rho)$  such that  $X = -\rho/(20R_p) + X_0$  where  $R_p$  is the planet's radius, and  $X_0$  is the obstacle stand off distance. Here  $\rho$  is the distance to the planet–star line, aberrated by an angle of  $\arctan(v_p/v_{sw})$  to account for the finite stellar wind speed relative to the planet's orbital speed. The shape of the obstacle is clearly seen in Fig. 1 that shows the protons and hydrogen atoms in a slice through the simulation domain.
- Elastic collision with another hydrogen atom, according to the DSMC method described in the next section.

All rates above are from Hodges<sup>2</sup> for Earth, and average solar conditions, scaled by  $(1/0.045)^2$  to account for the larger fluxes at HD 209458b. The photon-hydrogen collision rate,  $\tau_i$ , is chosen lower than a scaled value of  $0.6 - 1.6$  s<sup>-1</sup> over a solar cycle, to improve model fit. For the radiation pressure and photoionization event rates,  $\tau$ , after each time step, for each meta-particle, we draw a random time from an exponential distribution with mean  $\tau$ , and the event occur if this time is smaller than the time step. Note that we only consider ENAs produced outside the obstacle, so the fluxes presented here are a lower bound. Additional ENAs are produced inside, but including those would require a complete ion flow model.

The forces acting on a hydrogen atom are planetary gravity and the Coriolis force from the coordinate system rotating at an angular rate of  $\omega$ . The values of physical constants and parameters used in the simulation are listed in Table 1. Values of numerical parameters can be found in Table 2. The distribution of protons and hydrogen atoms in the simulation domain is illustrated in Figure 1. The total number of meta-particles at the final time is approximately  $8 \cdot 10^6$ .

## Collisions

The collisions between hydrogen atoms are modeled using the direct simulation Monte Carlo (DSMC) method<sup>3</sup>, where we divide the computational domain into cells. Then after each time step the particles that are in the same cells are considered for hard sphere collisions. From Bird<sup>3</sup> (Eq. 1.6), the frequency of collisions experienced by a single particle is  $\nu = n\sigma\overline{v_r}$ , where  $n$  is the total number density of all species,  $\sigma$  is the total collisional crosssection, and  $v_r$  is the relative velocity

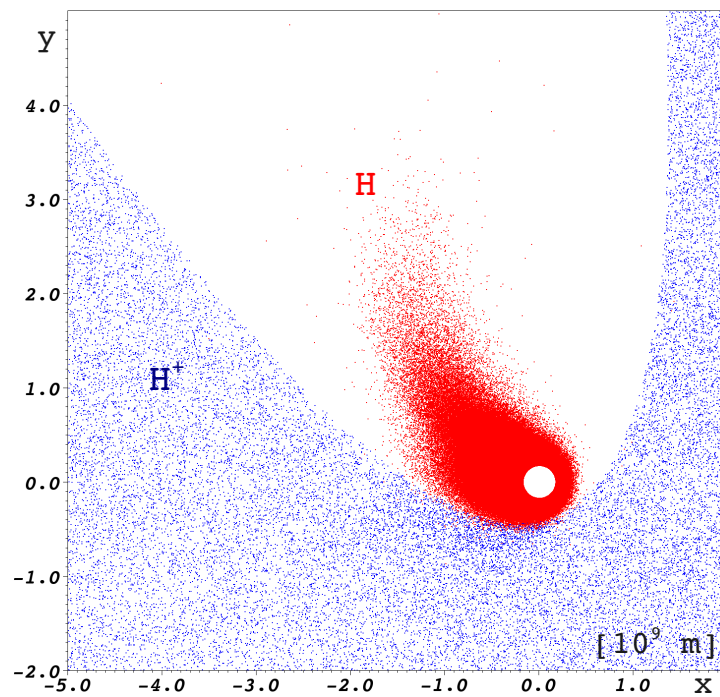


**Figure 1:** The flow of solar wind protons and the hydrogen exosphere cloud seen from above in the direction of the negative  $z$ -axis (perpendicular to the orbital plane). Each point corresponds to a neutral hydrogen (red), or a proton (blue) meta particle in the slice  $-10^8 \leq z \leq 10^8$  m. The circle without particles correspond to the inner boundary of the simulation, and the large area without protons corresponds to the assumed obstacle to the stellar wind, that is emptied of protons after each time step.

**Table 1:** Default values of physical parameters, and values of constants used in the simulations, unless otherwise noted.

Name	Symbol	Value
Star radius		$7.0 \cdot 10^8 \text{m}$
Planet radius	$R_p$	$9.4 \cdot 10^7 \text{m}$
Planet mass		$1.3 \cdot 10^{27} \text{kg}$
Orbital distance		$6.7 \cdot 10^9 \text{m}$
Orbital velocity		$1.4 \cdot 10^5 \text{m/s}$
Angular velocity	$\omega$	$2 \cdot 10^{-5} \text{rad/s}$
Inner boundary radius	$R_0$	$2 \cdot 10^8 \text{m}$
Inner boundary temperature		$0.7 \cdot 10^4 \text{K}$
Inner boundary density	$n$	$10^{14} \text{m}^{-3}$
H-H crossection		$10^{-21} \text{m}^2$
H-H <sup>+</sup> crossection (energy dependent <sup>5</sup> )		$\approx 2 \cdot 10^{-19} \text{m}^2$
UV absorption rate	$\tau_r$	$0.35 \text{s}^{-1}$
Photoionization rate	$\tau_i$	$7 \cdot 10^{-5} \text{s}^{-1}$
Obstacle standoff distance	$X_0$	$4 \cdot 10^8 \text{m}$
Solar wind density		$2 \cdot 10^9 \text{m}^{-3}$
Solar wind velocity	$u_{\text{sw}}$	$0.5 \cdot 10^5 \text{m/s}$
Solar wind temperature	$T_{\text{sw}}$	$1 \cdot 10^6 \text{K}$

between the particle and the particles in the surrounding gas. The bar denotes average. From this we get that the total collision frequency in a volume is

$$\frac{1}{2}n\nu = \frac{1}{2}n^2\overline{\sigma v_r} \quad (1)$$

For each pair of particles, their collision probability is proportional to  $\sigma v_r$ . For a cell, we estimate  $n$  by  $N_c N_m / V_c$  where  $N_c$  is the number of particles in the cell,  $N_m$  is the number of particles per meta-particle, and  $V_c$  is the cell volume. If  $N_m$  is different for different particles, we must sum all  $N_m$  instead of using  $N_c N_m$ .

To avoid an operation count proportional to  $N_c^2$ , following Garcia<sup>1</sup> (p. 359), we do not directly compute the averages. Instead we estimate a maximum value of  $\sigma v_r$ ,  $(\sigma v_r)_{\text{max}}$ , and use that in (1) to compute the number of trials. For each trial we then draw a random pair, and a random number  $R$  on  $[0, (\sigma v_r)_{\text{max}}]$ . If  $\sigma v_r > R$  for the chosen pair, the collision is accepted.

The random pair above is uniformly distributed if  $N_m$  is the same for all particles, as is the case for these simulations.

**Table 2:** Default numerical parameter values used in the simulations, unless otherwise noted.

Name	Symbol	Value
	$x_{\min}$	$-5 \cdot 10^9 \text{m}$
	$x_{\max}$	$2 \cdot 10^9 \text{m}$
	$y_{\min}$	$-7 \cdot 10^9 \text{m}$
	$y_{\max}$	$7 \cdot 10^9 \text{m}$
	$z_{\min}$	$-3.5 \cdot 10^9 \text{m}$
	$z_{\max}$	$3.5 \cdot 10^9 \text{m}$
Number of particles per meta-particle	$N_m$	$2.55 \cdot 10^{32}$
Number of cells		$16 \cdot 10^6$
Final time	$t_{\max}$	$10^5 \text{s}$
Time step	$\Delta t$	25 s

### Time integration

To avoid energy dissipation, the time advance of the particles from time  $t$  to time  $t + \Delta t$ , is done using the symplectic integrators derived by Candy and Rozmus<sup>4</sup>,

$$\begin{aligned}
 \mathbf{x} &\leftarrow \mathbf{x} + c_k \Delta t \mathbf{v}, \\
 \mathbf{a} &\leftarrow \mathbf{a}(\mathbf{x}, t), \\
 \mathbf{v} &\leftarrow \mathbf{v} + d_k \Delta t \mathbf{a}, \\
 t &\leftarrow t + c_k \Delta t,
 \end{aligned} \tag{2}$$

for  $k = 1, \dots, n$ . Here  $\mathbf{x}$  are the particle positions,  $\mathbf{v}$  the velocities, and  $\mathbf{a}(\mathbf{x}, t)$  the accelerations. The coefficients  $c_k$  and  $d_k$  can be found in Candy<sup>4</sup>. The global order of accuracy is  $n$ , and  $n = 2$  corresponds to the Leapfrog method. In this work we have used  $n = 4$ .

### Software

We use an existing software, FLASH, developed at the University of Chicago<sup>6</sup>, that provide adaptive grids and is fully parallelized, and that we have extended to do DSMC modeling of planetary exospheres<sup>7</sup>. FLASH is a general parallel solver for compressible flow problems. It is written in Fortran 90, well structured into modules, and open source. The parallelization is to a large extent handled by the PARAMESH<sup>8</sup> library that implements a block-structured adaptive cartesian grid with the Message-Passing Interface (MPI) library as the underlying communication layer.

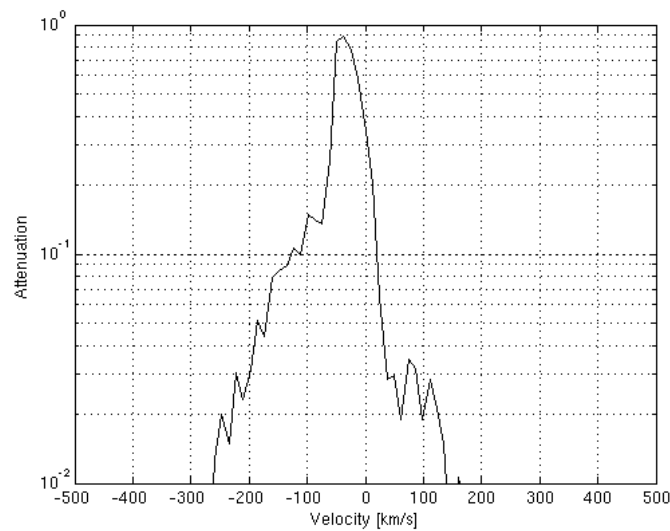


**Figure 2:** The computed attenuation at mid transit as a function of hydrogen  $x$ -axis velocity.

### Lyman-alpha attenuation

Given the positions of all the hydrogen meta particles at a certain time, we now proceed to compute how they attenuate the stellar Lyman-alpha radiation. We discretize the  $yz$ -plane using a grid. For each cell in the grid we compute the velocity spectrum of all hydrogen atoms in the column along the  $x$ -axis corresponding to the cell. We then subtract 13 km/s from the  $x$ -axis velocity of all atoms to account for the velocity of the star toward the Sun. This velocity spectrum can be converted into a frequency spectrum using the relation  $f = f_0 + v/\lambda_0$ , where  $v$  is the velocity,  $\lambda_0 = 1215.67 \cdot 10^{-8}$  cm, and  $f_0 = c/\lambda_0$ . This spectrum,  $h(f)$ , is normalized to have unit integral. Assuming only single scattering, the attenuation factor at each frequency is then

$$1 - e^{-ngfah(f)},$$

where  $n$  is the column density, the weighted oscillator strength  $gf = 2 \times 0.4162$ , and  $a = \pi e^2/(m_e c) = 0.026$  Hz cm<sup>2</sup>. This attenuation factor is then averaged over all columns in the  $yz$ -grid, except for those whose center fall outside the projected limb of the star, or inside the planet disc. The projected limb of the star is shifted downward (smaller  $z$ ) by  $4.58 \cdot 10^8$  m to account for the planet orbit's inclination. The computed attenuation is shown in Fig. 2, where we see that the separation between ENAs and exospheric hydrogen that was visible in the velocity spectrum also is apparent in the attenuation spectrum. This attenuation is then applied to the observed spectrum. At each velocity we simply multiply the observed spectrum by the attenuation factor.

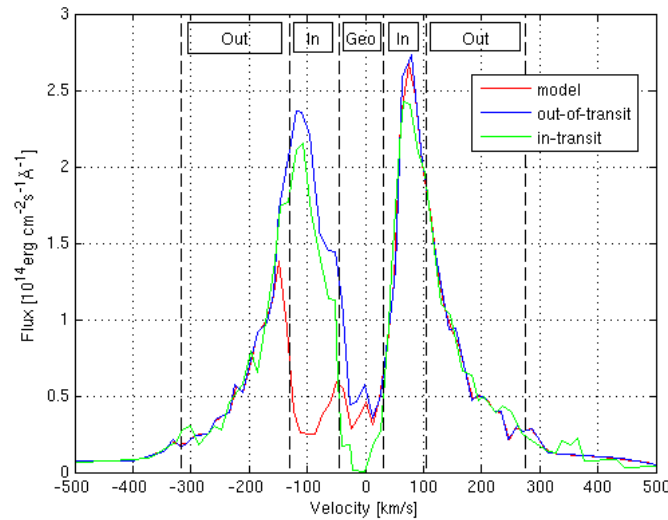


**Figure 3:** The attenuation spectrum with no ENA production and a larger radiation pressure corresponding to a photon collision rate of  $1.4 \text{ s}^{-1}$ .

### Parameter Dependence

Here we investigate the changes in the attenuation and velocity spectra when the values of some of the model parameters change.

First of all we turn off all ENA production and increase the radiation pressure. The resulting attenuation spectrum is shown in Fig. 3. We can see that the exospheric hydrogen now is accelerated up to velocities of  $-130 \text{ km/s}$ . However, the attenuation is too large, with a sharp drop off around  $-130 \text{ km/s}$ , as discussed in the paper.

Next we examine how the attenuation and velocity spectra change when the stellar wind velocity change. In Fig. 4 we show the effects of a  $100 \text{ km/s}$  stellar wind, and a  $0 \text{ km/s}$  stellar wind (as an extreme case of a surrounding plasma with no bulk velocity). For the faster stellar wind, the ENA part of the attenuation and velocity spectrum shift to larger negative velocities, while the slow stellar wind shift the spectra to positive velocities. This illustrates the possibility to estimate stellar wind velocity from observed attenuation spectra.

In Fig. 5 we see the resulting velocity spectrum when the stellar wind temperature is lower. The ENA part of the velocity spectrum is narrowed, showing the possibility to infer the stellar wind temperature from observations.

Increasing the inner boundary atmospheric temperature to  $8000 \text{ K}$  produces the attenuation spectrum shown in Fig. 6. The attenuation increases both in the red and blue part of the spectrum, since there is more atomic hydrogen available for charge exchange outside the obstacle.

Finally, in Fig. 7 we show the effect of moving the obstacle to the stellar wind (the magnetopause) further out to a distance of  $6 \cdot 10^8 \text{ m}$ . This reduces the attenuation in the red and blue

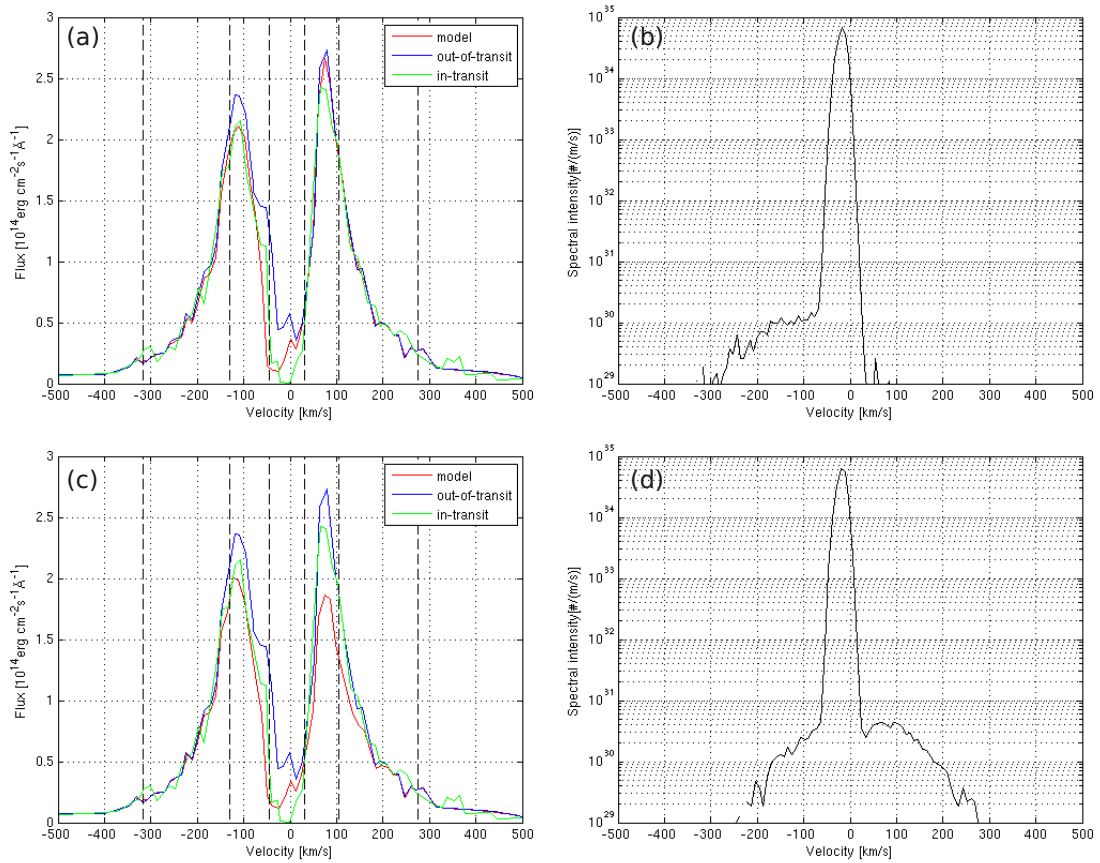


**Figure 4:** The attenuation spectrum (a) and velocity spectrum (b) for a 100 km/s stellar wind, and the attenuation spectrum (c) and velocity spectrum (d) for a 0 km/s stellar wind.

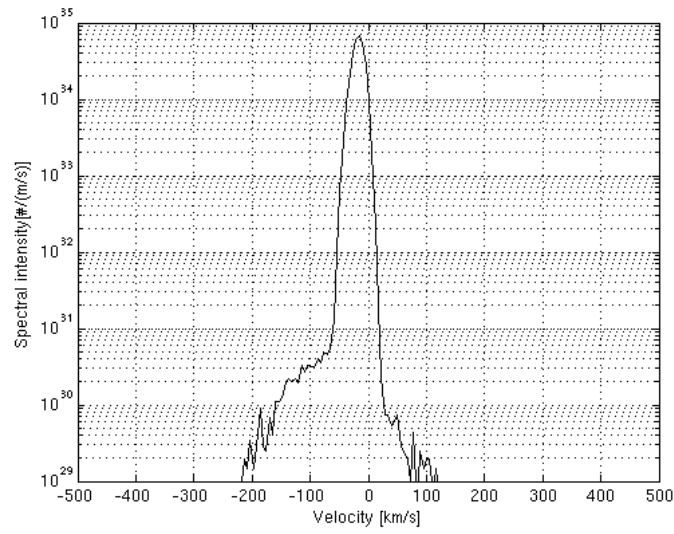


**Figure 5:** The velocity spectrum for a lower stellar wind temperature of  $0.5 \cdot 10^6$ .

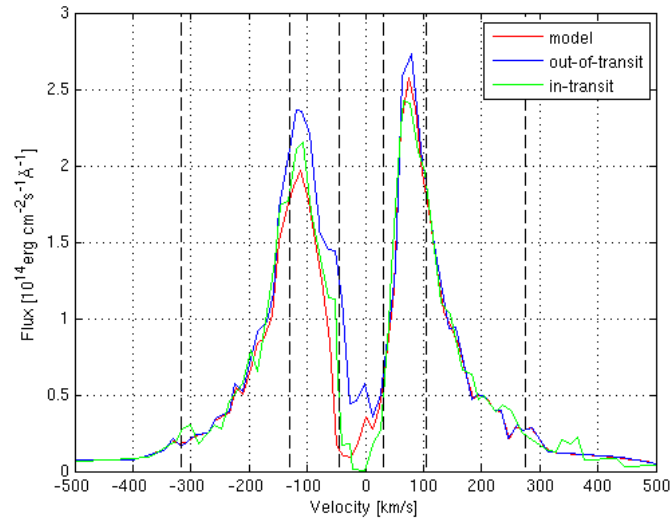


**Figure 6:** The attenuation spectrum for a higher atmospheric temperature of 8000 K at the inner boundary.

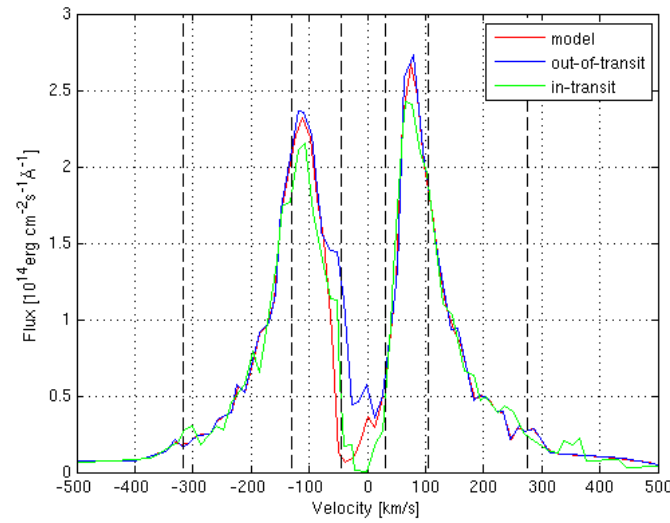


**Figure 7:** The attenuation spectrum for an increased obstacle distance of  $6 \cdot 10^8$  m.

part of the spectrum, since less exospheric hydrogen now is outside the obstacle.

## References

- [1] Garcia, A.L., Numerical Methods for Physics, 2nd edn, Prentice Hall, chap 11.3 (2000)
- [2] Hodges Jr., R.R., Monte Carlo simulation of the terrestrial hydrogen exosphere, *Journal of Geophysical Research*, 99, A12, 23,229-23,247 (1994)
- [3] Bird, G.A., *Molecular Gas Dynamics*, Clarendon Press (1976)
- [4] Candy, J., & Rozmus, W., A Symplectic Integration Algorithm for Separable Hamiltonian Functions, *Journal of Computational Physics*, 92, 230–256 (1991)
- [5] Lindsay, B. G. & Stebbings, R. F., Charge transfer cross sections for energetic neutral atom data analysis, *Journal of Geophysical Research*, 110, A12213 (2005)
- [6] Fryxell, B., et al., FLASH: An Adaptive Mesh Hydrodynamics Code for Modeling Astrophysical Thermonuclear Flashes, *The Astrophysical Journal Supplement Series*, 131, 273–334 (2000)
- [7] Holmström, M., Asymmetries in Mars' Exosphere: Implications for X-ray and ENA Imaging, *Space Science Reviews*, 126(1-4):435–445, 2006.
- [8] MacNeice, P., et al., PARAMESH : A parallel adaptive mesh refinement community toolkit, *Computer Physics Communications*, 126, 330– (2000)